Development of a new environmentally friendly and efficient centrifugal variable diameter metering device

Meng Zhang[1†], Pengfei Zhao[2†], Xiaojun Gao[2*] and Qinghui Lai[3]

[1]Faculty of Mechanical and Electrical Engineering, Kunming University of Science and Technology, Kunming, China, [2]College of Mechanical and Electronic Engineering, Northwest A&F University, Yangling, China, [3]Education Ministry Key Laboratory of Renewable Energy Advanced Materials and Manufacturing Technology, Yunnan Normal University, Kunming, China

Introduction: The design of the maize metering device involves centrifugal variable diameter pneumatic and cleaning mechanisms, aiming to enhance the performance and power efficiency of pneumatic maize metering devices. Leveraging the impact of changes in centrifugal diameter and the guidance and positioning of airflow, we optimize the hole insert, seeding plate, seed limit board, and integrated front shell. This optimization facilitates the adjustment of both the quantity and posture of seed filling. As a result, seeds can form a uniform flow within the annular cavity, reducing the wind pressure necessary for regular operation and decreasing power consumption.

Methods: A quadratic regression orthogonal rotation combination experiment is conducted using a self-made experiment bench, considering ground speed, wind pressure, and seeding rate as the experiment factors. Furthermore, a comparative experiment involving a novel centrifugal variable-diameter type metering device.

Results: The results indicate optimal seeding performance when the ground speed is 13.2 km/h, the wind pressure is 1.2 kPa, and the feeding rate is 25 seeds/s. Under these conditions, the quality of feed index reaches 95.20%, the multi-index is 3.87%, and the miss index is 0.93%. Findings reveal that the developed seed metering device achieved a quality of feed index exceeding 93.00% across varying speeds of 12~18 km/h, aligning with the production requirements. Moreover, the actual power consumption of Type B and C is about 85.00% and 98.00% lower than Type A, standing at only 32.90 W at 18 km/h. The COP of Type C is about 86 times and 12 times that of Type A and B, respectively, meeting the demands for efficient production of maize seed metering devices.

Discussion: In comparison to traditional design and structural parameter optimization methods for maize seed metering device, this study is helpful to the sustainable development of maize industry and reduce environmental pollution.

1 Introduction

Maize serves as a pivotal agricultural crop, contributing to animal feed, ethanol biofuels, and human consumption. Its significance lies in nourishing an expansive and burgeoning global population, albeit with the potential for pollution during production, impacting ecosystems and human health (Hill et al., 2019; Cisternas et al., 2020; Wei et al., 2023). Production methods are progressing towards greater efficiency and environmental cleanliness (Xiong et al., 2022). The primary objective of high-speed precision seeding technology is to ensure superior seeding quality while executing high-speed operations. The realization of this goal relies fundamentally on deploying a high-precision maize metering device (Li et al., 2021; Tang et al., 2022). Challenges such as population accumulation, squeezing, and friction among seeds impede seed-filling and substantially reduce seed-filling time, significantly impacting seed-filling performance. Moreover, the heightened velocity amplifies the centrifugal effect on seeds, exacerbating their instability within the seeding plate hole. Which is an influential factor constraining the swift evolution of precision seeding (Gao et al., 2022b). In response to the demands of efficient production, the structure of the maize metering device is progressively evolving into a more intricate form. However, this complexity increases work energy consumption. Regrettably, this trend is not aligned with the principles of clean and sustainable development in the maize industry (Bai et al., 2019; Zhu et al., 2022; Shah et al., 2023). Hence, the development of an efficient, sustainable, energy-saving, and emission-reducing seed-metering device emerges as pivotal for fostering the health of the maize industry.

Maize metering devices can be categorized into two types based on their operational principles: mechanical and pneumatic (Ren & Yi, 2022). The mechanical maize metering device relies solely on the seed's gravity for filling and clearing. Achieving the necessary accuracy at high speeds becomes challenging, with an increased risk of seed damage and low energy efficiency. This inability to adapt to the sustainable, clean production requirements of high-speed precision seeding is evident (Lei et al., 2021a; Du and Liu, 2023; Sun et al., 2023). In contrast, the pneumatic maize metering device showcases robust adaptability to seeds (Sun et al., 2020; Lei et al., 2021b; Li et al., 2023b). For example, Wang et al. (2021) designed an inside-filling maize metering device, investigating the correlation between ground speed and working wind pressure. Results indicated excellent seeding performance when the ground speed was 13.10 km/h and the working wind pressure was 4.75 kPa. Tang et al. (2023) proposed a pneumatic type of maize metering device. Results indicated optimal parameters, including a ground speed of 10 km/h and a wind pressure of 3 kPa in the tube. Wang et al. (2023) analyzed the high-speed sowing performance of three maize varieties at ground speeds exceeding 12 km/h. The results revealed the lowest miss index at negative pressures exceeding 6 kPa. Zhao et al. (2024) used numerical simulation and high-speed camera were employed to investigate the impact of diversion turbine structure, dynamic wind pressure, seed quantity, and ground speed on the air-assisted high-speed precision seeding system. Dong et al. (2024) designed a new type of perforated

precision seed metering device to improve the metering performance and energy efficiency of corn mechanical seed metering device under high-speed operation conditions, and the final performance coefficient was more significant than 9.2. Li et al. (2023a) designed a high-speed precision seed metering device for corn centrifugal grouting cleaning based on the principle of centrifugal force generated by the high-speed circular motion of seeds. Through response surface experiment optimization, it was found that the energy consumption during seeding is much lower than that of the air-suction seed metering device. Moreover, increasing the negative pressure improved the quality of feed index. Overall, it is evident that the working pressure of existing pneumatic maize metering devices exceeds 3 kPa, resulting in significant work energy consumption and a sharp increase in usage costs. Therefore, reducing the working pressure can effectively diminish production power consumption and contribute to the clean development of the maize industry.
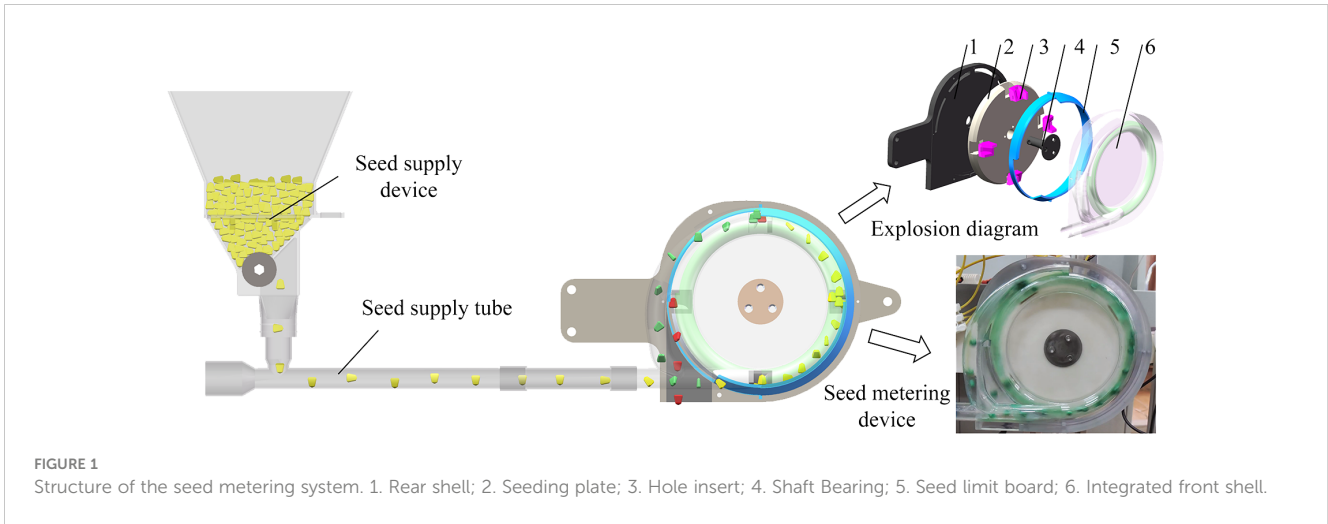
To achieve efficient and clean corn planting operations, this study introduces a novel pneumatic maize metering device leveraging the principles of centrifugal force and variable-diameter structure. The device comprises three essential components: the seed supply device, the supply tube, and the maize metering device, forming an annular cavity via the hole insert, seeding plate, seed limit board, and front shelf. Utilizing high-speed rotational operations, seeds are propelled regularly through the airflow and hole insert within the annular cavity, simultaneously generating centrifugal force. As the seed limit board's diameter abruptly changes, the typed hole insert collides with the seed limit board due to the centrifugal effect, disrupting the force chain among the seeds and altering their orientation in the hole insert to achieve optimal seed filling. To validate the performance and energy consumption of the seed metering device, a response surface test was conducted in a laboratory setting to evaluate the device's operational efficiency. Subsequently, comprehensive energy consumption comparisons were made through experiments with different maize metering devices, verifying the energy consumption of the new maize metering device using the coefficient of performance (COP) as the evaluation metric.

2 Materials and methods

The envisaged seed metering system is founded upon the governing principle of centrifugal force engendered by the circular trajectory of seeds. It predominantly comprises three integral components, as delineated in Figure 1. The seed metering device hinges upon the seed supply device and seed supply tube for the conveyance of seeds. The seeds descending from the seed supply device are systematically and uniformly propelled into the seed's primary filling area by the airflow originating from the seed supply tube, thereby orchestrating a seamless seed flow.
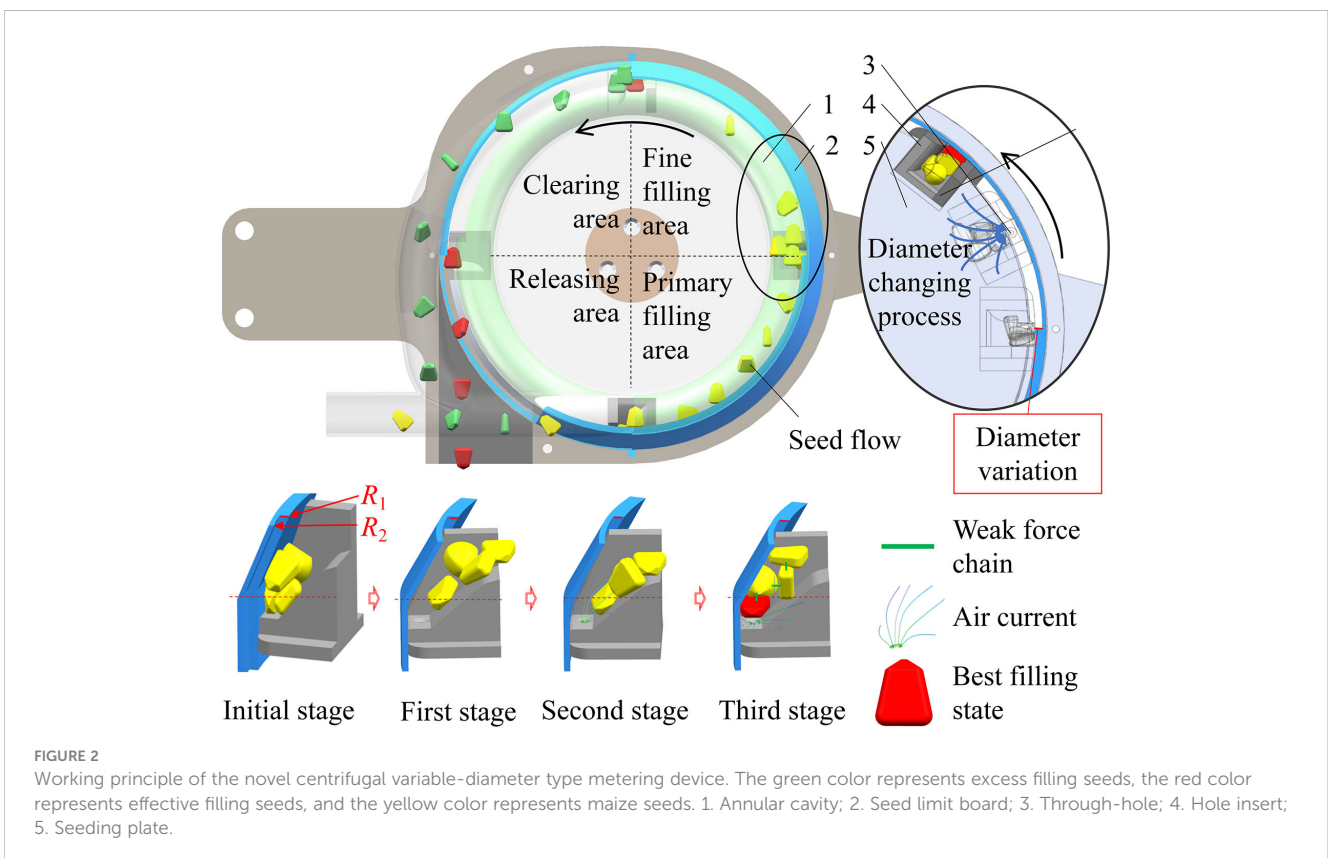
2.1 Seed metering device

According to the operational sequence of the seed metering device, the annular cavity undergoes a partition into the primary

FIGURE 1
Structure of the seed metering system. 1. Rear shell; 2. Seeding plate; 3. Hole insert; 4. Shaft Bearing; 5. Seed limit board; 6. Integrated front shell.

filling, fine filling, clearing, and releasing areas, as elucidated in Figure 2. In the primary filling area, the seeds accommodated within the hole insert rotate in the annular cavity. Subject to a more substantial centrifugal force, the groove for hole insert filling becomes susceptible to seed blockage or elevation. Therefore, in the fine filling area, bolstering the auxiliary airflow and modifying the thickness of the seed plate is imperative to ensure the quality of filling and accomplish stable grouting of individual seeds. This intricate process unfolds in three discernible stages. Initially, the interaction between the hole inserts and the seed limit board begets stimulating vibrations, disrupting the seed force chain within the

hole and inducing seed cluster disarray. Subsequently, airflow is discharged through the through-hole. With the efflux of airflow, seeds proximate to the through-hole at the bottom are directed downward and firmly pressed by the airflow, affecting guidance and positioning. This ensures optimal seed placement for precise single-seed filling. In the final stage, the seeds atop the hole insert undergo pressure from the seeds filled at the bottom. This enhances seed-carrying stability, facilitating the attainment of single-seed precision filling. During the clearing area, the protective space of the seed limit board diminishes, causing unsupported seeds to be expelled from the hole insert due to centrifugal force. After the solitary seed-

FIGURE 2
Working principle of the novel centrifugal variable-diameter type metering device. The green color represents excess filling seeds, the red color represents effective filling seeds, and the yellow color represents maize seeds. 1. Annular cavity; 2. Seed limit board; 3. Through-hole; 4. Hole insert; 5. Seeding plate.

releasing area, the constraint surface on the seed limit board vanishes. The seed, disengaging from the hole insert through centrifugal force, achieves single-grain precision seeding. To avert irregular movements of cleared seeds, influencing seeding performance, these removed seeds are thrust into the external reflux tube by centrifugal force and airflow. They then return methodically along the tube to the primary filling area, contributing to the subsequent cycle of seed filling. Its minimal power consumption during operation significantly diminishes production and utilization costs, fostering a cleaner seeding process.

2.2 Design of critical components

2.2.1 Front shell

The seeds seamlessly orchestrate a stable flow within the annular cavity, culminating in meticulously executing the filling, clearing, and releasing processes. The front shell, depicted in Figure 3, encompasses key components such as a seed inlet, an annular cavity, a reflux tube, and a seed outlet. In a strategic move to curtail air consumption and seed rebound, the central region of the front shell is isolated. Simultaneously, an external reflux tube is ingeniously integrated to preempt the issues of reseeding seed rebound arising from the erratic movement of cleared seeds within the annular cavity. Ensuring a systematic reintroduction of cleared seeds into the primary filling area, this design also safeguards against the direct flow of airflow from the inlet tube to the reflux tube. The inner diameter is meticulously determined, ensuring it does not surpass the diameter of the inlet tube while forming an acute angle with it. In practical operations, the inner diameter of the annular cavity tube is calibrated to accommodate the hole insert, settled at 0.02 m. The inner diameters of the inlet tube and the reflux tube are harmonized with the annular cavity tube to avert airflow reflux, all fixed at 0.02 m, with a reflux angle β set at 45°.

The cleaning duration is compressed during high-speed operations, often resulting in the ineffective removal of surplus seeds. Hence, it becomes imperative to design the cleaning outlet's

position meticulously. The board's width is deliberately reduced in the clearing area, causing excess seeds to lose support from the board. Subject to the influence of centrifugal force, the seed undergoes a primary detachment from the hole insert, followed by a streamlined throwing motion. During high-speed operation, the centrifugal force exerted on the seed significantly surpasses that of gravity, warranting the dismissal of gravity's influence. The seeding plate's rotation angle (δ) upon seed separation from the hole insert can be calculated using its motion equation, elegantly illustrated in Equation 1.

$$\delta = \sqrt{\frac{2L_1}{r}} \qquad (1)$$

It can be seen from Equation 1 that the rotation angle (δ) when the seed is separated from the mold hole is only determined by the variable (L_1), the distance, and the radius (r) of the seed hole insert. Remarkably, this angle remains independent of the rotation speed. Consequently, alterations in ground speed will not induce changes in the cleaning point's position. Following meticulous calculations, the angle (δ) is estimated to be approximately 30°. The cleaning port of the reflux tube is strategically positioned at the tangent of the cleaning point, forming an angle (λ) of 60°.

2.2.2 Hole insert

The hole insert comes into direct contact with the seed, rendering its structural form and parameters pivotal in shaping its performance. As shown in Figure 4.

The contact area between the reclined position of seeds and the specific hole is maximized, offering a relatively stable posture conducive to efficient filling. Hence, a higher proportion of reclined postures during filling corresponds to superior seeding performance, as depicted in Figure 5A. The hole must accommodate three to five seeds to ensure the primary filling effect. Influenced by centrifugal force, the seeds above the hole exert pressure, covering the seeds within the effective filling area at the hole's base. However, an excess of seeds poses challenges for clearing. Therefore, the critical dimensions of the hole insert should
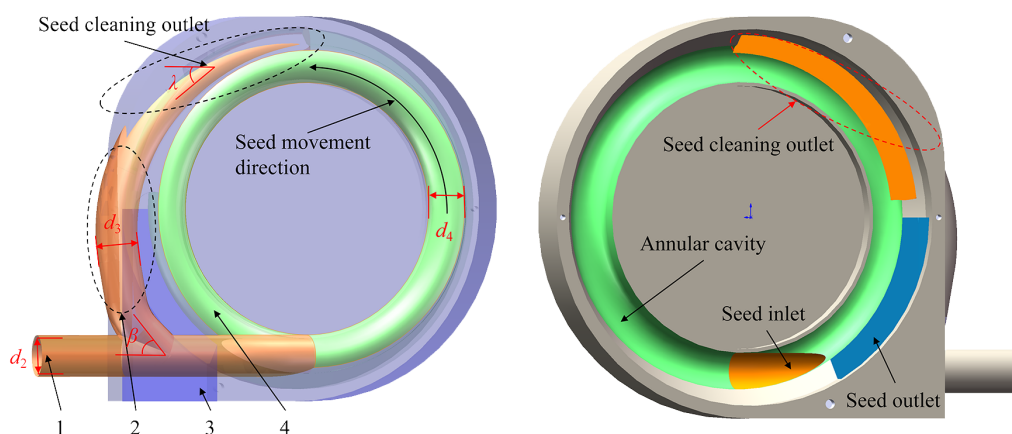

FIGURE 3
Sectional view of the front shell. 1. Seed inlet; 2. Reflux tube; 3. Seed outlet; 4. Annular cavity.
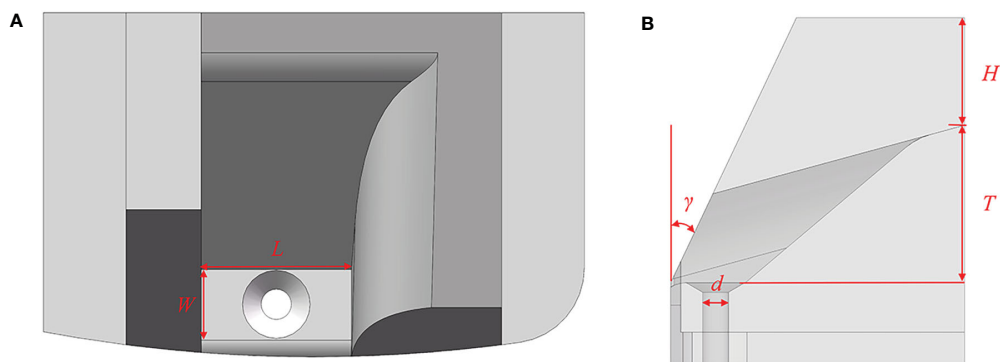
FIGURE 4
Hole insert schematic diagram. **(A)** Top view; **(B)** Perspective view.
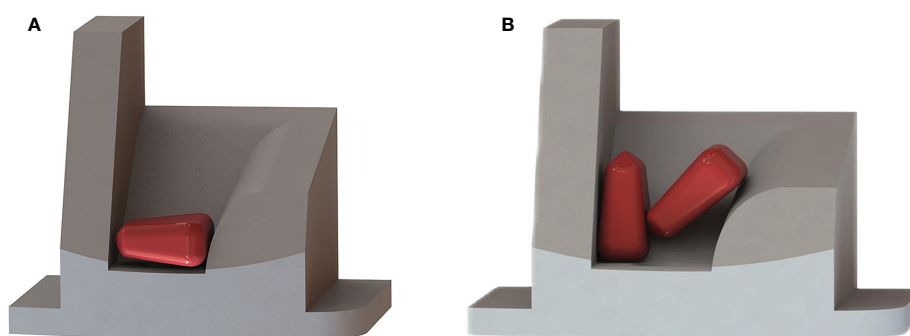

FIGURE 5
The different states of the seed in the hole insert. **(A)** Ideal filling posture; **(B)** Schematic of seeds jamming.

satisfy the following Equation 2:

$$\begin{cases} l_0 < L < l_0 + t_0 \\ w_0 < W < w_0 + t_0 \\ l_0 < T < 1.5l_0 \\ H > 0.5l_0 \end{cases} \qquad (2)$$

After careful deliberation, the hole L, W, T, and H dimensions are chosen as 0.012, 0.009, 0.012, and 0.008 m, respectively. In collaboration with the seed limit board to facilitate the seamless sliding of seeds into the hole, the γ is set at 30°.

Owing to the diverse shapes and substantial differences in size across the three axes, they intertwine during the filling process, leading to frequent irregular clustering of multiple seeds at the hole's base—a situation prone to jamming, as shown in Figure 5B. Consequently, following the completion of the primary filling process, the seed orientation within the effective filling area undergoes adjustment to a singular reclined posture through variable-diameter and airflow-guided positioning. The seeds at the hole were positioned through the pressure generated by turbulence resistance (Kabeel et al., 2019). So, a through-hole is incorporated at the bottom of the hole insert to achieve airflow guidance and precise positioning. Research has determined that the chamfered through-hole exhibited a wide range of airflow, which facilitates the adjustment of seed orientation (Li et al., 2021).

Consequently, the chamfered through-hole has been chosen for this study. Proximate to the through-hole, seeds gradually encounter airflow, enabling dynamic adjustment of their orientation and position during this process. Following the design manual of agricultural machinery, select a through-hole with a diameter (d) of 0.004 m (Ji et al., 2018).

2.2.3 Seeding plate

The seeding plate serves as a rotating component, propelling seeds in a rapid circular motion. A sliding groove is incorporated into the seeding plate to achieve the centrifugal variable diameter feature of the hole insert, as illustrated in Figure 6.

The duration of the filling process directly impacts the success rate of sowing. The plate's diameter significantly influences the performance and dimensions upon determining the hole number. Nevertheless, an excessive diameter for the seeding plate may result in increased dimensions, manufacturing costs, and assembly challenges for the seeding device. Referring to the investigations conducted by Gao et al. (2023), which featured a seeding plate with four-hole inserts, the diameter is conclusively established as 0.20 m.

2.2.4 Seed limit board

The seed limit board is crucial in achieving variable-diameter single-grain fine filling, ensuring precision in seeding, and seamlessly integrating with the hole insert. Specifically, the radius

FIGURE 6
Schematic diagram of the seeding plate structure.
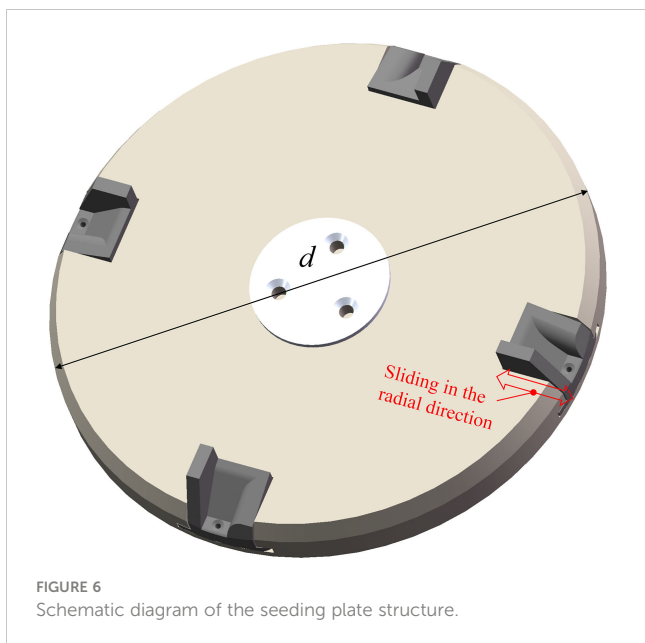
R_2 (large arc) of the seed limit board in the primary filling area is larger than the radius R_1 (small arc) in the fine filling area. A radial mutation occurs at the junction between the seed limit board in the primary filling area and the seed limit board in the fine filling area. Its primary function is to expel the insert from the hole, allowing seeds experiencing excessive pressure during the primary filling process to loosen.

The seed limit board incorporates a gradient curve structure, facilitating the gradual repositioning of the hole insert to its original state. Guided by the contour curve, the structural configuration of the seed limit board is meticulously determined, involving essential parameters such as the front width W_1 in the primary filling and fine filling areas, the front width W_2 in the cleaning area, the width W_3 in the releasing area, the front angle α, the radial mutation length l_1, the small arc radius R_1, and the large arc radius R_2. A collaborative synergy unfolds between the seed limit board and the hole insert in the intricate seed-filling process. After thorough consideration, the W_1, W_2, W_3, α, and l_1 are determined as 0.017

m, 0.006 m, 0.010 m, 30°, and 0.003 m, respectively. The R_1 is set at 0.101 m to harmonize with the seed limit board, while the maximum R_2 reaches 0.104 m, as illustrated in Figure 7.

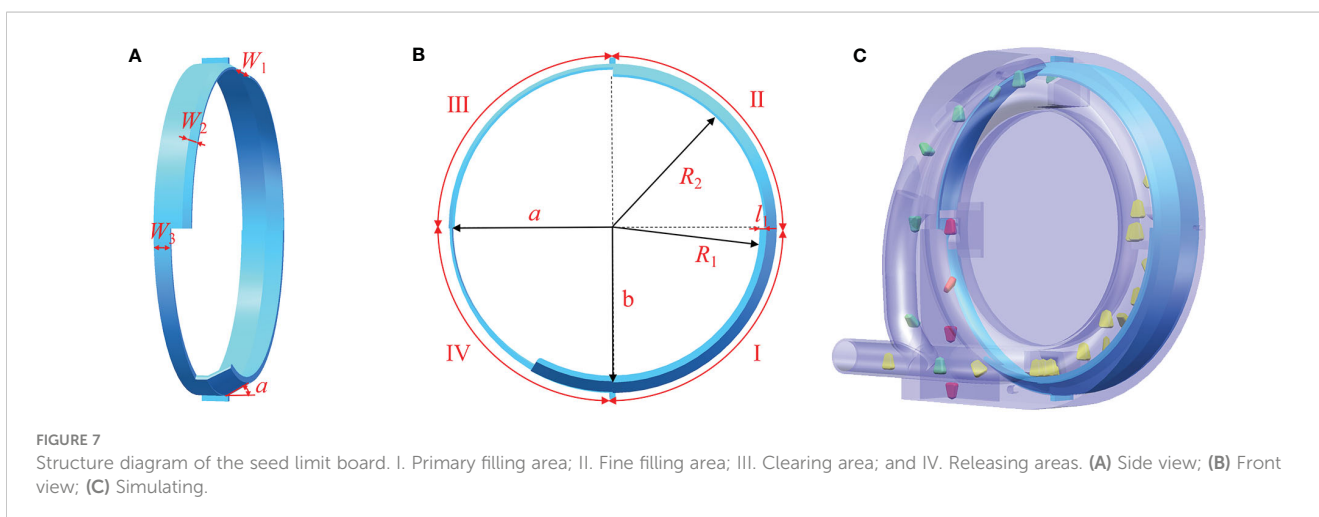## 2.3 Experiments and methods

2.3.1 Experimental bench

We meticulously engineer an experimental bench to evaluate the consumption of seeding performance and substantiate the efficacy and superiority of the proposed maize metering device. This experimental bench includes a seed metering system, a high-speed camera (HF Agile Device Co., Ltd., China), two motors, and two motor controllers, showcased in Figure 8. The seeding system underwent trial production utilizing 3D printing technology and cost-effective resin materials. Zhengdan-958 maize (ungraded) seeds are utilized in the experiment, maintaining a plant spacing of 0.30 m during seeding (Gao et al., 2020).

2.3.2 Response surface experiment of CCD

The quality of the metering device lies in its high-speed adaptability across varying ground speeds. Furthermore, the pneumatic metering device's wind pressure significantly influences the velocity of seeds within the apparatus, and maintaining an appropriate seed-feeding rate is crucial for sustaining the dynamic equilibrium. The optimal interplay among the factors mentioned is pivotal for achieving high-speed precision seeding devices. Consequently, the experimental factors encompass ground speed (X_1), wind pressure (X_2), and feeding rate (X_3). Adhering to the international standard ISO 7256/1, each experiment involves sowing 500 seeds. Equation 3 below presents the formula for computing these experimental indicators.

$$\begin{cases} Y_1 = \frac{n_1}{N'} \times 100\,\% \\ Y_2 = \frac{n_2}{N'} \times 100\,\% \\ Y_3 = \frac{n_0}{N'} \times 100\,\% \end{cases} \quad (3)$$

where Y_1 denotes the quality of feed index, %; Y_2 denotes the multi-index, %; Y_3 denotes the miss index, %; n_1 denotes the

FIGURE 7
Structure diagram of the seed limit board. I. Primary filling area; II. Fine filling area; III. Clearing area; and IV. Releasing areas. **(A)** Side view; **(B)** Front view; **(C)** Simulating.
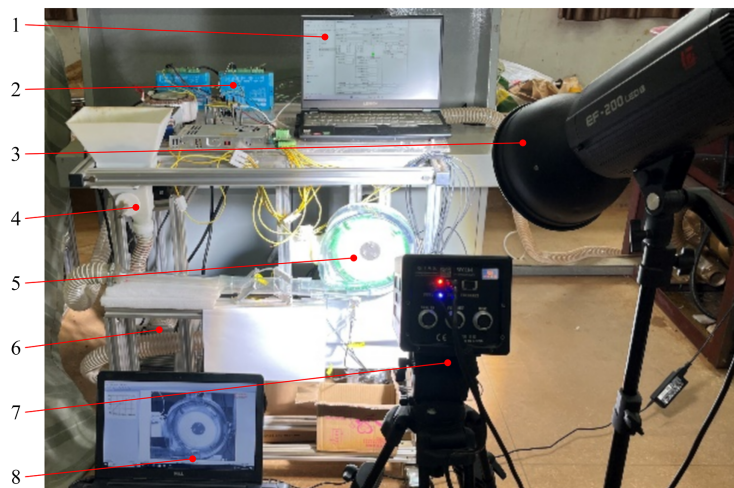
FIGURE 8
The experimental bench. 1. PC to control the seed metering device; 2. Motor controller; 3. Fill light; 4. Seed feeding device; 5. Seed metering device; 6. Turbine blower; 7. High-speed camera; 8. PC to control the high-speed camera.

number of seeds normally sown; n_2 denotes the number of multiples; n_0 denotes the number of misses; N' denotes the number of intervals.

Response surface experiments are pivotal in assessing factors' influence on performance (Gao et al., 2021; Liu et al., 2023; Kadam and Pawade, 2024). The experiments encompassed three factors at five levels. The experimental design process and the subsequent result processing are carried out using Design-Expert 13 (Stat-Ease, Minneapolis, Minnesota, USA). A regression analysis is also performed to ascertain the optimal operational parameters, as shown in Table 1.

2.3.3 Performance and energy efficiency experiments

Maintaining optimal wind pressure is crucial for ensuring the efficient and regular operation of the pneumatic planter. Reduced wind pressure lowers production energy consumption and enhances energy efficiency, enabling low-energy and clean production. A comparative analysis is conducted with similar centrifugal seed metering devices to elucidate the power consumption of the novel centrifugal variable-diameter pneumatic seeding device, as depicted in Figure 9. Notably, Type

A represents a high-speed centrifugal filling-cleaning precision seed metering device. It utilizes a diversion turbine to disrupt the seed population, ensuring optimal filling, and employs an internal reflux replication scheme for seed reflow refilling (Zhao et al., 2024). Type B represents the previous generation of the centrifugal variable diameter pneumatic seed metering device. It relies on a distinctive variable diameter structure for optimal filling and utilizes an external reflux tube for reflow refilling the cleaned seeds (Gao et al., 2022a). Type C represents the novel centrifugal variable-diameter type metering device designed. It reduces the inner diameter of the annular tube and increases the turning radius of the reflux tube. The performance, power consumption, and COP of three distinct types of centrifugal filling-cleaning seed metering devices are assessed under optimal operating conditions, corresponding to ground speeds of 12, 14, 16, and 18 km/h. The power needed to generate wind pressure can be computed using Equation 4, and the COP can be determined using Equation 5.

$$P = \frac{1}{4}\pi d_a^2 v_a p \tag{4}$$

$$COP = \frac{A}{P} \tag{5}$$

where P is the power required to generate wind pressure (kW), d_a is the diameter of the airflow tube opening (m), v_a is the air velocity (m/s), and p is the wind pressure (kPa).

3 Results and discussion

3.1 Analysis of variance

Table 2 displays the results of the laboratory bench experiment. Subsequently, distinct mathematical models are formulated linking ground speed, wind pressure, and feeding rate with the different

TABLE 1   Levels of the experimental factors.

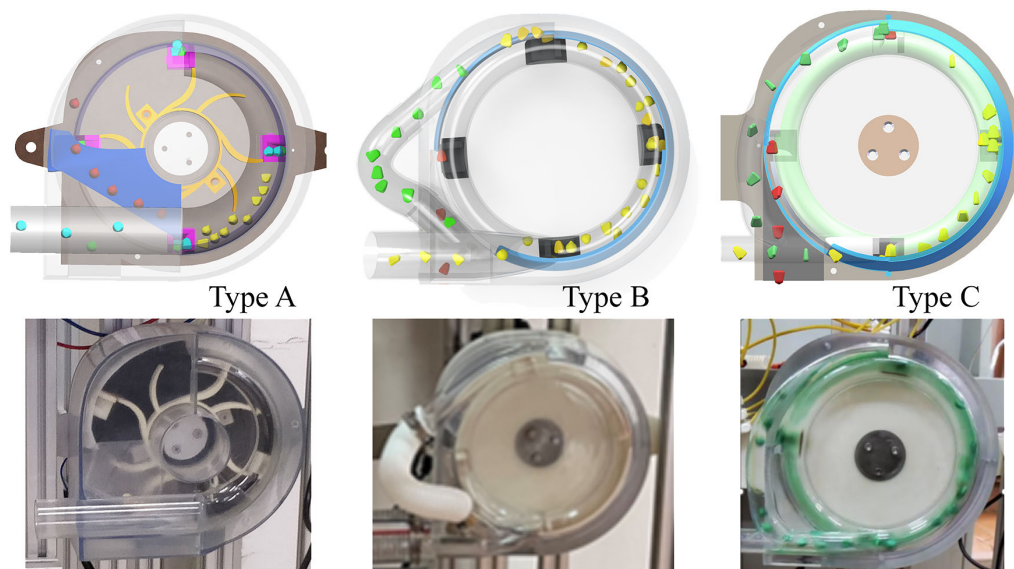| Level	Factors		
	Ground speed X_1 (km/h)	Wind pressure X_2 (kPa)	Feeding rate X_3 (seeds/s)
-1.682	12.0	1.0	10
-1	12.8	1.0	14
0	14.0	1.5	20
1	15.2	1.8	26
1.682	16.0	2.0	30

FIGURE 9
The experimental seed metering devices. The d_a of Type A is 0.043 m; the d_a of Type B is 0.036 m; the d_a of Type C is 0.020 m.

indexes. Linear regression equations for Y_1, Y_2, and Y_3 are derived individually. Following the elimination of non-significant factors, the regression equation for the quality of feed index is formulated, as illustrated in Equation 6.

$$Y_1 = 93.27 - 0.95X_1 - 0.95X_2 + 1.01X_3 + 0.57X_1X_2 - 1.30X_1{}^2 - 0.82X_2{}^2 - 0.93X_3{}^2$$
$$Y_2 = 5.31 + 0.50X_1 + 0.56X_2 - 0.53X_3 - 0.79X_1X_2 + 1.02X_1{}^2 + 0.77X_2{}^2 + 0.40X_3{}^2$$
$$Y_3 = 1.45 + 0.46X_1 + 0.39X_2 - 0.48X_3 + 0.32X_1X_3 + 0.38X_2X_3 + 0.27X_1{}^2 + 0.53X_3{}^2$$

$$(6)$$

The variance analysis quality of the feed index experiment data is conducted using the software. The significance of the experiment results for the regression equation is presented in Table 3. A P-value less than 0.05 for the model suggests its significance. A lack-of-fit P-value exceeding 0.1 implies insignificance in the lack of fit. The impact of each factor on the quality of feed index, ranked from largest to smallest, is X_3, X_1, and X_2. The influence of each factor on the multi-index, from largest to smallest, is X_2, X_3, and X_1. Among these, the first-order terms (X_1, X_2, X_3), the interaction term (X_1X_2), and the quadratic term ($X_1{}^2$, $X_2{}^2$, $X_3{}^2$) significantly affect Y_1 and Y_2, while the others are not significant. The influence of various factors on the miss index is ranked from largest to smallest: X_3, X_1, and X_2. The first-order terms (X_1, X_2, X_3), the interaction terms (X_1X_3, X_2X_3), and the quadratic terms ($X_1{}^2$, $X_3{}^2$) significantly affect the miss index, while the others are not significant.

3.2 Response analysis of the experimental factors

Figures 10, 11, 12A, D display the surface and contour drawings illustrating the impact of the interaction term X_1X_2 on the different

indexes at X_3 of 20 seeds/s. The centrifugal force of the seed increases as the X_1 increases, leading to an enhanced filling effect. Nevertheless, when the X_1 exceeds 14.0 km/h, excessive centrifugal pressure is applied to the seeds, compressing more than one seed at the bottom and impeding effective removal during the cleaning process. This leads to a reduction in Y_1. Conversely, when the X_2 exceeds 1.5 kPa, the inlet velocity of seeds rises due to high wind pressure, causing some seeds to be unable to fill into the hole insert and be discharged directly. This leads to a reduction in Y_1. When X_3 is 20 seeds/s, maintaining the X_2 between 1.2~1.5 kPa and the X_1 between 12.8~14.0 km/h, the Y_1 can be upheld above 93.00%.

Figures 10, 11, 12B, E depict the surface and contour drawings illustrating the influence of the interaction term X_1X_3 on the different indexes when the X_2 is 1.5 kPa. In cases where the X_1 and X_3 are both low, fewer seeds are in the hole insert, leading to a lower Y_1. Conversely, with high X_1 and low X_3, excessive centrifugal force intensifies the impact vibration effect on the hole at the variable diameter position of the seed limit board. Consequently, the seeds initially filled in the hole insert become prone to detachment, leading to a lower Y_1. When the X_1 and X_3 are high, numerous seeds get compressed at the bottom. The cleaning process, however, fails to effectively eliminate the excess seeds, leading to a decline in Y_1. When X_2 is 1.5 kPa, maintaining the X_3 between 20~26 seeds/s and the X_1 between 12.8~14.0 km/h, the Y_1 can be sustained at levels above 93.00%.

Figures 10, 11, 12 C, F depict the surface and contour drawings illustrating the influence of the interaction term X_2X_3 on the different indexes when the X_1 is 14.0 km/h. When X_2 and X_3 are both low, fewer seeds are filled into the hole insert, and the airflow is weak, leading to lower Y_1 and Y_2, and Y_3 is the opposite. When the X_3 is low and the X_2 is high, it leads to a poor filling effect and, consequently, a

TABLE 2 Experimental scheme and results.

No.	Factors			Performance indexes		
	X_1 (km/h)	X_2 (kPa)	X_3 (seeds/s)	Y_1 (%)	Y_2 (%)	Y_3 (%)
1	12.8	1.2	14	90.93	6.27	2.80
2	15.2	1.2	14	88.53	8.54	2.93
3	12.8	1.8	14	89.33	8.14	2.53
4	15.2	1.8	14	88.53	8.80	2.67
5	12.8	1.2	26	94.13	5.07	0.80
6	15.2	1.2	26	90.67	8.00	1.33
7	12.8	1.8	26	90.13	8.67	1.20
8	15.2	1.8	26	89.60	6.93	3.47
9	12.0	1.5	20	91.33	7.33	1.33
10	16.0	1.5	20	87.87	8.93	3.20
11	14.0	1.0	20	92.80	6.53	0.67
12	14.0	2.0	20	89.07	8.27	2.67
13	14.0	1.5	10	88.67	7.60	3.73
14	14.0	1.5	30	92.60	5.13	2.27
15	14.0	1.5	20	93.87	5.33	0.80
16	14.0	1.5	20	92.27	6.13	1.60
17	14.0	1.5	20	93.20	5.07	1.73
18	14.0	1.5	20	92.40	5.93	1.67
19	14.0	1.5	20	94.00	4.87	1.13
20	14.0	1.5	20	94.93	4.13	0.93
21	14.0	1.5	20	93.20	5.07	1.73
22	14.0	1.5	20	93.07	5.53	1.40
23	14.0	1.5	20	92.53	5.73	1.93

lower Y_1. When the X_3 and X_2 are high, the occurrence of seeds falling directly from unfilled holes increases, resulting in a decrease in the Y_1. With X_1 at 14 km/h, maintaining the X_2 between 1.20 and 1.50 kPa, and X_3 between 20 and 26 seeds/s, Y_1 can surpass 93.00%.

3.3 Parameter optimization

The response surface graph indicates an optimum value for the seeding. Utilizing regression equations, the optimal combination of X_3, X_2, and X_1 for seeding performance can be determined by optimizing the Y_1, Y_2, and Y_3. The optimization objectives include achieving the lowest Y_2 and Y_3 and the highest Y_1. Conducting a multi-factor optimization solution on the established quadratic regression model is performed under specified boundary conditions, with constraint conditions outlined as illustrated in Equation 7.

$$\begin{cases} \max Y_1(x_1, x_2, x_3) \\ \min Y_2(x_1, x_2, x_3) \\ \min Y_3(x_1, x_2, x_3) \\ 12\,\text{km/h} \le x_1 \le 16\,\text{km/h} \\ 1\,\text{kPa} \le x_2 \le 2\,\text{kPa} \\ 10\,\text{seeds/s} \le x_3 \le 30\,\text{seeds/s} \end{cases} \quad (7)$$

Design-Expert calculations deduce that the highest seeding performance occurred at X_1 of 13.2 km/h, X_2 of 1.2 kPa, and X_3 of 25 seeds/s. Under these conditions, the Y_1, Y_2, and Y_3 are 94.45%, 5.02%, and 0.53%, respectively. Bench experiments are conducted under identical conditions to validate the accuracy of the optimal solution. The bench experiment results demonstrated that Y_1, Y_2, and Y_3 are 95.20%, 3.87%, and 0.93%, respectively. These values closely align with the optimal solution, affirming their high reliability.

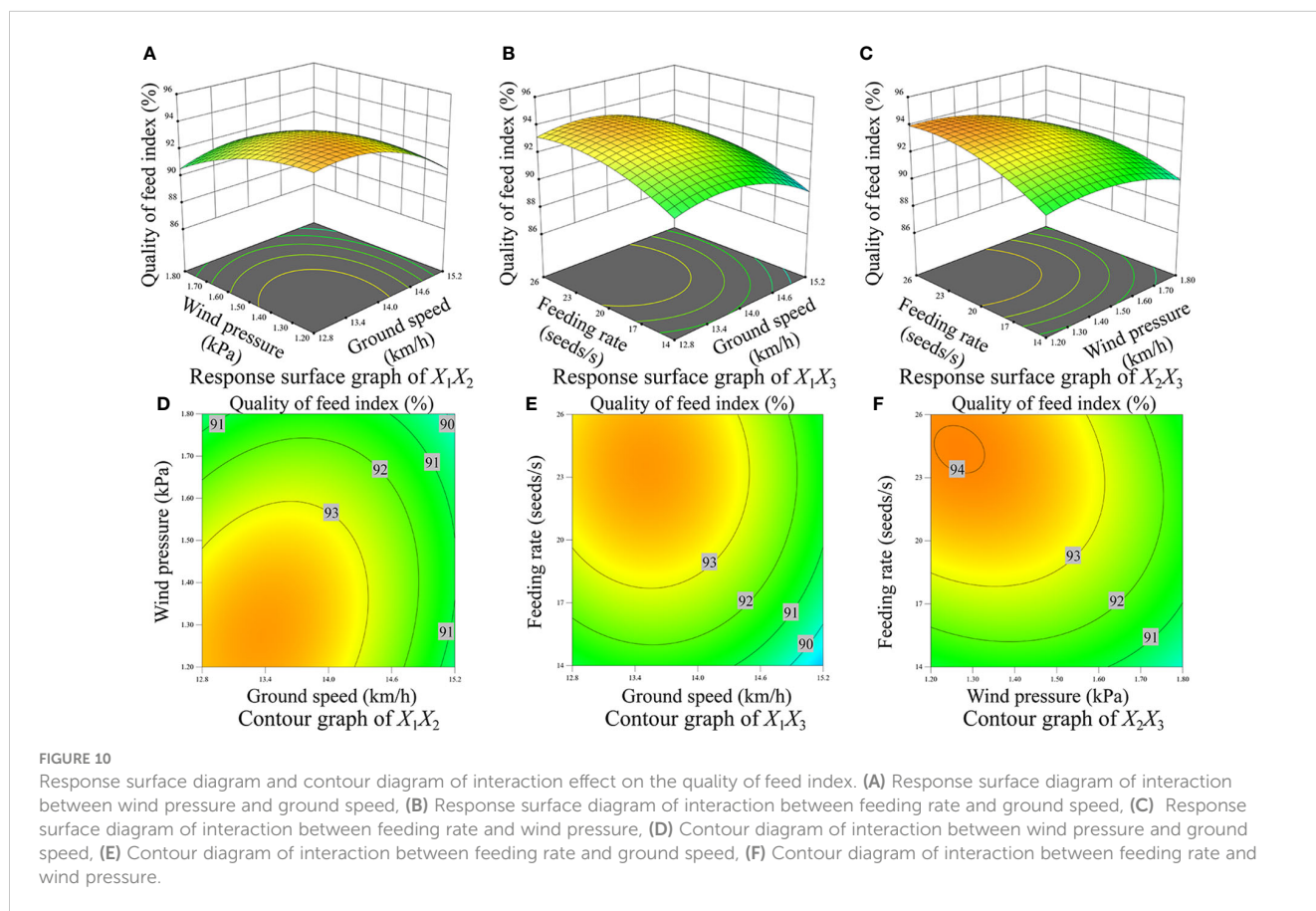## 3.4 Performance and energy efficiency comparison results

3.4.1 Operation performance

The seeding performance of three distinct centrifugal seed metering devices at varying ground speeds is detailed in Table 4. Evidently, the novel centrifugal variable-diameter type metering device effectively harnesses the centrifugal force generated during high-speed operation, exhibiting superior performance under optimal working conditions and ensuring Y_1 exceeds 93.00%. Among these, the Type A seed metering device attains a higher wind pressure and Y_2 under identical conditions. In the operation process, the metering device's internal cavity relies on the wind pressure and the guide turbine structure to adjust the seed posture, and there is no airflow tube inside, so a large wind pressure is needed to ensure the wind pressure inside the whole metering device. At the same time, under the combined action of a larger wind pressure and a high-speed rotating diversion turbine structure, it is easy to make the seeds filled in the cavity directly discharged from the seed outlet so that the Y_2 increases. Furthermore, seeds cleaned in the clearing area collide with the inclined baffle during the falling process, inducing irregular seed movement and increasing the Y_2. The Type B seed metering device exhibits a relatively low Y_1 and significant Y_2 and Y_3. The diameter of the annular seed tube in the seed metering device is large, which leads to the seeds not being filled with the hole insert directly ejected from the releasing area, and the Y_2 is improved. Additionally, seeds cleaned in the clearing area, influenced by centrifugal force during the reflux tube, experience substantial inertial motion. The inadequate turning radius of the reflux tube is prone to blockages during reflux, diminishing the seed supply and subsequently elevating the Y_3. The Type C seed metering device is optimized based on Types A and B. Compared to the Type A device, its Y_3 increases, attributed to the collision strength between the hole insert and the seed limit board during the diameter-changing process. While this collision may lead to occasional miss-seeding, it aligns with the seed metering device's design requirements. Regarding Y_1 and Y_2, Type C outperforms Type B across all metrics, requiring the least wind pressure and better aligning with cleaner production operational requirements.

TABLE 3 Results of the analysis of variance for quadratic models.

Source	Y_1		Y_2		Y_3	
	F-value	P-value	F-value	P-value	F-value	P-value
Mode	19.92	<0.0001**	14.03	<0.0001**	11.36	<0.0001**
X_1	23.80	0.0003**	9.53	0.0087**	17.94	0.0010**
X_2	23.56	0.0003**	11.82	0.0044**	13.41	0.0029**
X_3	26.86	0.0002**	10.75	0.0060**	20.15	0.0006**
X_1X_2	4.93	0.0448*	13.83	0.0026**	2.43	0.1431
X_1X_3	0.15	0.7049	1.06	0.3216	5.08	0.0422*
X_2X_3	2.89	0.1129	0.056	0.8165	7.47	0.0171*
X_1^2	51.24	<0.0001**	46.80	<0.0001**	7.35	0.0178*
X_2^2	20.71	0.0005**	26.20	0.0002**	0.36	0.5595
X_3^2	26.39	0.0002**	7.16	0.0191*	28.31	0.0001**
Lack of fit	0.204	0.9517	0.8855	0.5323	1.40	0.3188

* represents $P< 0.05$, indicating that the model term is significant, while ** represents $P< 0.01$, indicating that the model term is extremely significant.

FIGURE 10
Response surface diagram and contour diagram of interaction effect on the quality of feed index. **(A)** Response surface diagram of interaction between wind pressure and ground speed, **(B)** Response surface diagram of interaction between feeding rate and ground speed, **(C)** Response surface diagram of interaction between feeding rate and wind pressure, **(D)** Contour diagram of interaction between wind pressure and ground speed, **(E)** Contour diagram of interaction between feeding rate and ground speed, **(F)** Contour diagram of interaction between feeding rate and wind pressure.

3.4.2 Operation energy efficiency

In Figure 13A, the power of each type at different ground speeds is illustrated, with the power ranking as Type A, Type B, and Type C from large to small. The power of all seed metering devices increases with the increase in ground speed, but the power consumption of Type A devices increases more obviously. In addition, the power consumption of Type A is significantly higher than that of Types B and C. The air annular tube design in the metering device cavity significantly reduces the required air pressure. The actual power consumption of Types B and C is about 85.00% and 98.00% lower than that of Type A, respectively, indicating that a suitable air annular tube helps similar metering devices reduce power
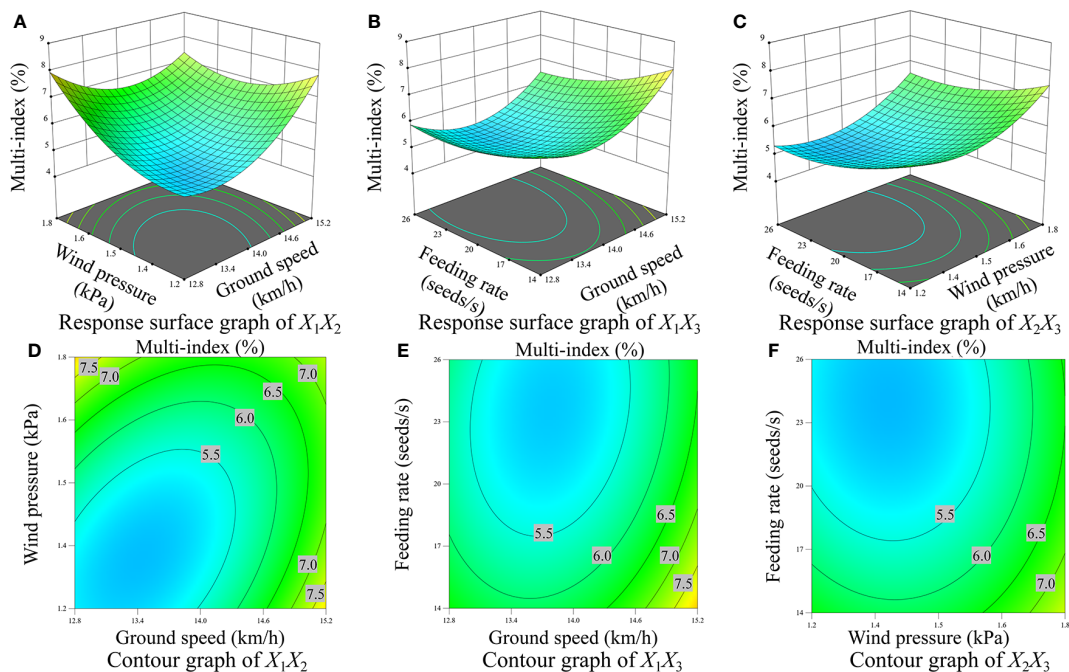
FIGURE 11
Response surface diagram and contour diagram of interaction effect on the multi-index. **(A)** Response surface diagram of interaction between wind pressure and ground speed, **(B)** Response surface diagram of interaction between feeding rate and ground speed, **(C)** Response surface diagram of interaction between feeding rate and wind pressure, **(D)** Contour diagram of interaction between wind pressure and ground speed, **(E)** Contour diagram of interaction between feeding rate and ground speed, **(F)** Contour diagram of interaction between feeding rate and wind pressure.
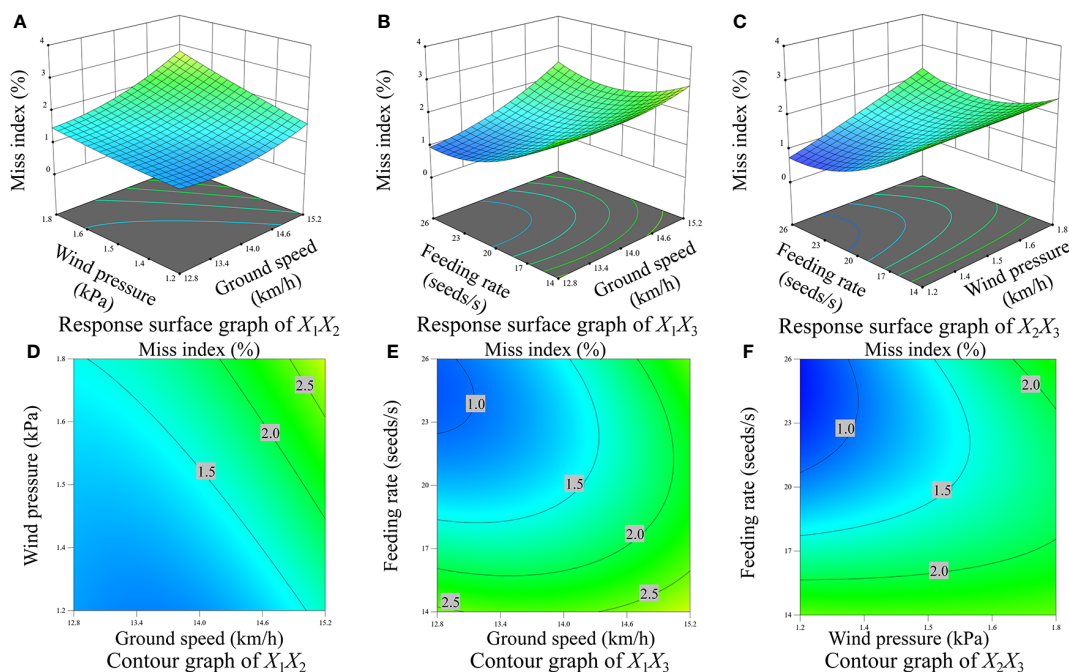

FIGURE 12
Response surface diagram and contour diagram of interaction effect on the miss index. **(A)** Response surface diagram of interaction between wind pressure and ground speed, **(B)** Response surface diagram of interaction between feeding rate and ground speed, **(C)** Response surface diagram of interaction between feeding rate and wind pressure, **(D)** Contour diagram of interaction between wind pressure and ground speed, **(E)** Contour diagram of interaction between feeding rate and ground speed, **(F)** Contour diagram of interaction between feeding rate and wind pressure.
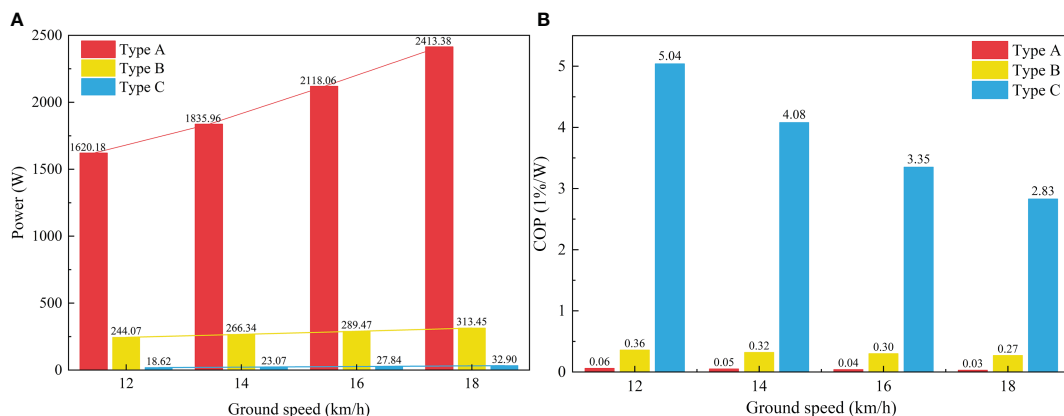
FIGURE 13
Comparison results of energy efficiency. **(A)** Power of seed metering devices; **(B)** COP of seed metering devices.

consumption. The COP of each type of seed metering device at different ground speeds is presented in Figure 13B, where Type C, Type B, and Type A follow the sequence from large to small. The COP of Type C is about 86 times and 12 times that of Types A and B, respectively. The changing trend contrasts with power, with COP values decreasing as ground speed increases. The Type C seed metering device attains a higher COP value, signifying that the seed metering device designed excels in energy efficiency and is well-suited for maize's efficient and clean production needs.

4 Conclusion

This study introduces a novel centrifugal variable-diameter metering device. The proposed seed metering device features a

simpler structure and lower production costs. It requires only a small airflow during the operation process, leading to low energy consumption and a higher energy utilization rate, aligning more closely with the development trend of efficient and clean maize production.

(1) A novel centrifugal variable-diameter type metering device has been meticulously designed. The centrifugal diameter-changing effect and airflow-guided positioning facilitate the achievement of single-grain precision filling. The cleared seeds are systematically refilled through the outer filling of the shell, enabling high-speed precision seeding operations. The structure is streamlined, resulting in a simpler design and a significantly lower production cost.

(2) The regression orthogonal rotation combination experiment uses the self-built experiment platform. The response surface method is employed to elucidate the impact of each factor on the experiment index. The optimal seeding performance is achieved when the ground speed is 13.2 km/h, the wind pressure is 1.2 kPa, and the refilling amount is 25 seeds/s. During this optimal condition, the quality of feed index reaches 95.20%, the multi-index is 3.87%, and the miss index is 0.93%.

(3) The performance, power consumption, and COP of the maize metering device developed are compared and analyzed. The results reveal that the quality of feed index of the developed novel centrifugal precision metering device exceeds 93.00% at a ground speed of 12~18 km/h, meeting the requirements of high-speed operation. In addition, the actual power consumption of Types B and C is about 85.00% and 98.00% lower than that of Type A. The COP of Type C is about 86 times and 12 times that of Types A and B, respectively. This implies that a judicious combination of a reasonable annular cavity diameter and centrifugal diameter change effect can ameliorate the augmented energy efficiency and more effectively cater to clean production requirements.

TABLE 4 The experiment results of different types of seed metering devices.

Type	X_1 (km/h)	X_2 (kPa)	Speed of the plate (rpm)	Y_1 (%)	Y_2 (%)	Y_3 (%)
Type A	12	9.2	166.67	90.35	8.91	0.74
	14	10.0	194.44	90.17	9.30	0.53
	16	11.3	222.22	90.47	8.86	0.67
	18	12.0	250.00	90.6	8.93	0.47
Type B	12	3.3	166.67	86.8	6.13	7.07
	14	3.5	194.44	86.13	7.74	6.13
	16	3.7	222.22	87.33	7.27	5.40
	18	3.9	250.00	85.52	8.72	5.76
Type C	12	1.3	166.67	93.87	5.46	0.67
	14	1.5	194.44	94.15	4.67	1.18
	16	1.7	222.22	93.36	5.38	1.26
	18	1.9	250.00	93.21	5.26	1.53

Data availability statement

The raw data supporting the conclusions of this article will be made available by the authors, without undue reservation.

Author contributions

MZ: Conceptualization, Investigation, Writing – original draft. PZ: Investigation, Software, Writing – original draft. XG: Methodology, Writing – review & editing. QL: Conceptualization, Methodology, Resources, Writing – original draft, Writing – review & editing.

Conflict of interest

The authors declare that the research was conducted in the absence of any commercial or financial relationships that could be construed as a potential conflict of interest.

Publisher's note

All claims expressed in this article are solely those of the authors and do not necessarily represent those of their affiliated organizations, or those of the publisher, the editors and the reviewers. Any product that may be evaluated in this article, or claim that may be made by its manufacturer, is not guaranteed or endorsed by the publisher.

References

Bai, Y., Deng, X., Jiang, S., Zhao, Z., and Miao, Y. (2019). Relationship between climate change and low-carbon agricultural production: A case study in Hebei Province, China. *Ecol. Indic.* 105, 438–447. doi: 10.1016/j.ecolind.2018.04.003

Cisternas, I., Velasquez, I., Caro, A., and Rodriguez, A. (2020). Systematic literature review of implementations of precision agriculture. *Comput. Electron. Agric.* 176, 105626. doi: 10.1016/j.compag.2020.105626

Dong, J., Zhang, S., Zheng, Z., Wu, J., Huang, Y., and Gao, X. (2024). Development of a novel perforated type precision metering device for efficient and cleaner production of maize. *J. Cleaner Product.* 443, 140928. doi: 10.1016/j.jclepro.2024.140928

Du, X., and Liu, C. (2023). Design and testing of the filling-plate of inner-filling positive pressure high-speed seed-metering device for maize. *Biosyst. Eng.* 228, 1–17. doi: 10.1016/j.biosystemseng.2023.02.008

Gao, X., Cui, T., Zhou, Z., Yu, Y., Xu, Y., Zhang, D., et al. (2021). DEM study of particle motion in novel high-speed seed metering device. *Adv. Powder Technol.* 32, 1438–1449. doi: 10.1016/j.apt.2021.03.002

Gao, X., Xie, G., Li, J., Shi, G., Lai, Q., and Huang, Y. (2023). Design and validation of a centrifugal variable-diameter pneumatic high-speed precision seed-metering device for maize. *Biosyst. Eng.* 227, 161–181. doi: 10.1016/j.biosystemseng.2023.02.004

Gao, X., Xie, G., Xu, Y., Yu, Y., and Lai, Q. (2022a). Application of a staggered symmetrical spiral groove wheel on a quantitative feeding device and investigation of particle motion characteristics based on DEM. *Powder Technol.* 407, 117650. doi: 10.1016/j.powtec.2022.117650

Gao, X., Zhao, P., Li, J., Xu, Y., Huang, Y., and Wang, L. (2022b). Design and experiment of quantitative seed feeding wheel of air-assisted high-speed precision seed metering device. *Agriculture* 12, Article 11. doi: 10.3390/agriculture12111951

Gao, X., Zhou, Z., Xu, Y., Yu, Y., Su, Y., and Cui, T. (2020). Numerical simulation of particle motion characteristics in quantitative seed feeding system. *Powder Technol.* 367, 643–658. doi: 10.1016/j.powtec.2020.04.021

Hill, J., Goodkind, A., Tessum, C., Thakrar, S., Tilman, D., Polasky, S., et al. (2019). Air-quality-related health damages of maize. *Nat. Sustainab.* 2, 397–403. doi: 10.1038/s41893-019-0261-y

Ji, Y., Liu, S., and Li, J. (2018). Experimental and numerical studies on dense-phase pneumatic conveying of spraying material in venturi. *Powder Technol.* 339, 419–433. doi: 10.1016/j.powtec.2018.08.031

Kabeel, A. E., Elkelawy, M., Bastawissi, H. A. E., and Elbanna, A. M. (2019). An experimental and theoretical study on particles-in-air behavior characterization at different particles loading and turbulence modulation. *Alexandria Eng. J.* 58, 451–465. doi: 10.1016/j.aej.2019.04.002

Kadam, G. S., and Pawade, R. S. (2024). Water vapor cutting fluid assisted productive machining of Inconel 718. *Mat. Manufact. Processes* 39, 98–109. doi: 10.1080/10426914.2023.2190389

Lei, X., Hu, H., Wu, W., Liu, H., Liu, L., Yang, W., et al. (2021a). Seed motion characteristics and seeding performance of a centralised seed metering system for rapeseed investigated by DEM simulation and bench testing. *Biosyst. Eng.* 203, 22–33. doi: 10.1016/j.biosystemseng.2020.12.017

Lei, X., Hu, H., Yang, W., Liu, L., Liao, Q., and Ren, W. (2021b). Seeding performance of air-assisted centralized seed-metering device for rapeseed. *Int. J. Agric. Biol. Eng.* 14, 79–87. doi: 10.25165/j.ijabe.20211405.5349

Li, J., Lai, Q., Zhang, H., Zhang, Z., Zhao, J., and Wang, T. (2021). Suction force on high-sphericity seeds in an air-suction seed-metering device. *Biosyst. Eng.* 211, 125–140. doi: 10.1016/j.biosystemseng.2021.08.031

Li, C., Cui, T., Zhang, D., Yang, L., He, X., Li, Z., et al. (2023a). Design and experiment of a centrifugal filling and cleaning high-speed precision seed metering device for maize. *J. Cleaner Product.* 426, 139083. doi: 10.1016/j.jclepro.2023.139083

Li, H., Ling, L., Wen, C., Liu, H., Wu, G., An, X., et al. (2023b). Structural optimization method of rice precision direct seed-metering device based on multi-index orthogonal experimental. *Front. Plant Sci.* 14, 1183624. doi: 10.3390/agriculture12081094

Liu, X., Niu, Z., Li, M., Hou, M., Wei, L., Zhang, Y., et al. (2023). Design and experimental research on disc-type seeding device for single-bud sugarcane seeds. *Int. J. Agric. Biol. Eng.* 16, 115–124. doi: 10.25165/j.ijabe.20231602.6973

Ren, S., and Yi, S. (2022). Control Mechanism and experimental study on electric drive seed metering device of air suction seeder. *Tehnicki Vjesnik* 29, 1254–1261. doi: 10.17559/TV-20210908053555

Shah, W. U. H., Lu, Y. T., Liu, J. H., Rehman, A., and Yasmeen, R. (2023). The impact of climate change and production technology heterogeneity on China's agricultural total factor productivity and production efficiency. *Sci. Total Environ.* 907, 168027. doi: 10.1016/j.scitotenv.2023.168027

Sun, J., Chen, H., Duan, J., Liu, Z., and Zhu, Q. (2020). Mechanical properties of the grooved-wheel drilling particles under multivariate interaction influenced based on 3D printing and EDEM simulation. *Comput. Electron. Agric.* 172, 105329. doi: 10.1016/j.compag.2020.105329

Sun, X., Niu, L., Cai, M., Liu, Z., Wang, Z., and Wang, J. (2023). Particle motion analysis and performance investigation of a fertilizer discharge device with helical staggered groove wheel. *Comput. Electron. Agric.* 213, 108241. doi: 10.1016/j.compag.2023.108241

Tang, H., Xu, F., Guan, T., Xu, C., and Wang, J. (2023). Design and test of a pneumatic type of high-speed maize precision seed metering device. *Comput. Electron. Agric.* 211, 107997. doi: 10.1016/j.compag.2023.107997

Tang, H., Xu, C., Wang, Z., Wang, Q., and Wang, J. (2022). Optimized design, monitoring system development and experiment for a long-belt finger-clip precision corn seed metering device. *Front. Plant Sci.* 13, 814747. doi: 10.3390/agriculture12081094

Wang, J., Qi, X., Xu, C., Wang, Z., Jiang, Y., and Tang, H. (2021). Design evaluation and performance analysis of the inside-filling air-assisted high-speed precision maize seed-metering device. *Sustainability* 13, 5483. doi: 10.3390/su13105483

Wang, C., Yang, H., He, J., Kang, K., and Li, H. (2023). The influence of seed variety and high seeding speed on pneumatic precision seed metering. *Engenharia Agrícola* 43, e20220183. doi: 10.1590/1809-4430-eng.agric.v43n3e20220183/2023

Wei, H. H., Zhang, K. P., Chai, N., Wang, Y., Li, Y. L., Yang, J., et al. (2023). Exploring low-carbon mulching strategies for maize and wheat on-farm: Spatial responses, factors and mitigation potential. *Sci. Total Environ.* 906, 167441. doi: 10.1016/j.scitotenv.2023.167441

Xiong, L., Shah, F. R., and Wu, W. (2022). Environmental and socio-economic performance of intensive farming systems with varying agricultural resource for maize production. *Sci. Total Environ.* 850, 158030. doi: 10.1016/j.scitotenv.2022.158030

Zhao, P., Gao, X., Su, Y., Xu, Y., and Huang, Y. (2024). Investigation of seeding performance of a novel high-speed precision seed metering device based on numerical simulation and high-speed camera. *Comput. Electron. Agric.* 217, 108563. doi: 10.1016/j.compag.2023.108563

Zhu, Y., Zhang, Y., and Piao, H. (2022). Does agricultural mechanization improve the green total factor productivity of China's planting industry? *Energies* 15, 940. doi: 10.3390/en15030940